Sp8 is crucial for limb outgrowth and neuropore closure

Sheila M. Bell*, Claire M. Schreiner, Ronald R. Waclaw, Kenneth Campbell, S. Steven Potter†, and William J. Scott†

Division of Developmental Biology, Cincinnati Children's Hospital Medical Center, 3333 Burnet Avenue, Cincinnati, OH 45229

Edited by Mario R. Capecchi, University of Utah, Salt Lake City, UT, and approved August 20, 2003 (received for review July 10, 2003)

In this report we describe the developmental expression and function of Sp8, a member of the Sp family of zinc finger transcription factors, and provide evidence that the *legless* transgene insertional mutant is a hypomorphic allele of the *Sp8* gene. *Sp8* is expressed during embryogenesis in the forming apical ectodermal ridge (AER), restricted regions of the central nervous system, and tail bud. Targeted deletion of the *Sp8* gene gives a striking phenotype, with severe truncation of both forelimbs and hindlimbs, absent tail, as well as defects in anterior and posterior neuropore closure leading to exencephaly and spina bifida. Outgrowth of the limb depends on formation of the AER, a signaling center that forms at the limb bud apex. In *Sp8* mutants, the AER precursor cells are induced and initially express multiple appropriate marker genes, but expression of these genes is not maintained and progression to a mature AER is blocked. These observations indicate that Sp8 functions downstream of Wnt3, Fgf10, and Bmpr1a in the signaling cascade that mediates AER formation.

apical ectodermal ridge | exencephaly | spina bifida | zinc finger | *legless*

Outgrowth of the vertebrate limb requires the formation and maintenance of the apical ectodermal ridge (AER) at the distal limb bud margin. The initial induction of the murine AER precursor cells requires canonical Wnt signaling through ectodermal expression of *Wnt3* (1), ectodermal Bmp signaling (2), and the interaction of Fgf10 expressed by the limb mesoderm with its receptor Fgfr2b expressed in the limb ectoderm (3–5). The induced AER precursor population of cells is initially localized on the ventral surface of the emerging murine limb bud and expresses several specific markers, including *Fgf8* (6, 7). With subsequent growth, this population of cells becomes localized at the ventro-distal margin of the limb bud before constricting to form a mature AER.

The progression of the AER precursor into a definitive AER is poorly understood. It has been observed, however, that a disruption of this process occurs in the *legless* (*lgl*) transgene insertional mutant. In *lgl* mutant hindlimbs, the AER precursor cells are induced, but fail to localize at the ventro-distal limb margin and an AER subsequently fails to form (6). In contrast, in the forelimbs, an AER does form, but with irregularities in the anterior margin. These observations correlate well with the *lgl* homozygous mutant limb phenotype, with the hindlimbs missing all structures distal to the femur and with variable loss of distal-anterior forelimb structures (8, 9). Other aspects of the *lgl* mutant phenotype include randomized left–right axis formation, missing olfactory bulbs, encephalocoeles or exencephaly, and cleft lip. Previous studies showed that both the zinc finger transcription factor *Sp4* and the left right dynein (*Lrd*) genes (10, 11) are deleted by the *lgl* transgene insertion, but gene targeting results indicated that neither gene is responsible for the limb truncation or craniofacial malformations observed in *lgl* mutants (Fig. 1*A*).

Release of the human genome sequence revealed the presence of a second zinc finger transcription factor gene, *Sp8*, in a region syntenic to the *lgl* transgene insertion on mouse chromosome 12. This gene was of particular interest because of its homology to the *Drosophila D-Sp1* gene, implicated in leg development (12). In mammals, seven other Sp family members have been described (for review see ref. 13). All Sp proteins possess a highly conserved DNA-binding domain comprised of three Cys2His2 zinc fingers that interact with GC and GT boxes commonly found within the promoter regions of genes. Targeted mutations of mouse *Sp1*, *3*, *4*, *5*, and *7* have previously been reported. Absence of the ubiquitously expressed *Sp1*gene results in embryo lethality at embryonic day 10 (E10) (14). *Sp3*-deficient mice die at birth of respiratory failure and have delayed bone ossification and impaired tooth development (15, 16). Targeted disruption of *Sp4* results in a reduction in viability and growth, cardiac malformations, and a failure of males to mate (10, 17). No overt phenotype is observed in *Sp5* null mice (18), whereas *Sp7* (*osterix*) mutants show a striking inability to form bone (19).

In this report we describe the expression and function of the *Sp8* gene. In the developing limbs *Sp8* showed restricted expression in the ectoderm, including the AER precursor cells. Of further interest, in *lgl* mice the *Sp8* coding sequences are intact, but the gene showed reduced levels of expression, particularly in the developing hindlimbs, suggesting an *Sp8* hypomorphic allele. Consistent with this, mice with a targeted deletion of *Sp8* gave a dramatic phenotype including the absence of tails and severely truncated forelimbs and hindlimbs. CNS defects included a failure to close both the anterior and posterior neuropores, leading to exencephaly and spina bifida. Molecular analysis showed that *Sp8* is not necessary for induction of the AER precursor, but is required for its maintenance and maturation into a definitive AER.

Methods

Gene Targeting. The targeting vector was generated by using a Cre/lox targeting vector in which the neomycin resistance gene is immediately flanked by Frt sequences. 5′ to *Neo* is a unique *Fse1* site, a *loxP* sequence, and a unique *Pme1* site. Sequences 3′ to *Neo* include a second *loxP* sequence and a unique *Srf1* site. The following *Sp8* gene specific primers were used to PCR amplify genomic regions for subcloning into each of these sites. A 4.2-kb fragment was amplified by using the primers 5′-ATTGCCCGGGCCCCAGCACCAAAACTGCCT-3′ and 5′-ATTGCCCGGGCTCCCCCTCAACCCATCCTTA-3′ and subcloned into the *Srf1* site. A 2.1-kb fragment was amplified by using the primers 5′-TTAAGTTTAAACGGGGAGAAGCAACTAAGGA-3′ and 5′-TTAAGTTAAACCAAGGATTCAGCCACCGATG-3′ and subcloned into the *Pme1* site. A 3.6-kb fragment was amplified by using the primers 5′-TAAGGCCGGCCGACAGTAAGTAGCACACAT-3′ and 5′-TAAGGCCGGCGATAAAGAAGCCAGGAGAAA-3′ and subcloned into the *Fse1* site. Mice were generated from R1ES cells carrying the modified allele and were bred to either black

This paper was submitted directly (Track II) to the PNAS office.

Abbreviations: AER, apical ectodermal ridge; E*n*, embryonic day *n*.

*To whom correspondence should be addressed. E-mail: sheila.bell@cchmc.org.

†S.S.P. and W.J.S. contributed equally to this work.

DEVELOPMENTAL BIOLOGY

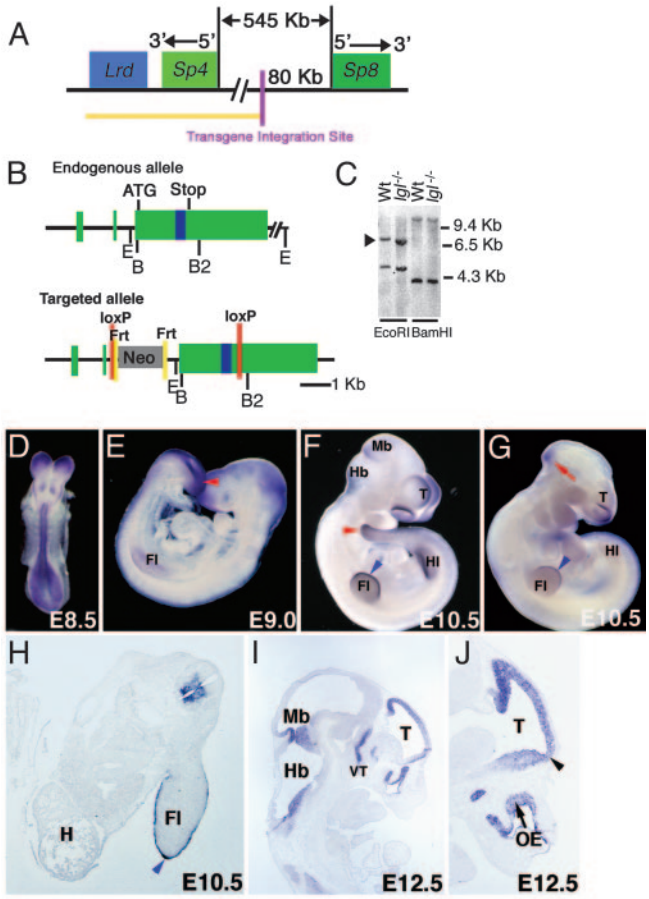

Fig. 1. Structural characterization and expression of the *Sp8* gene. (*A*) Relationship between the *Sp8* and *Sp4* genes. Yellow line indicates genomic region known to be deleted in the *lgl* transgene insertional mutant. (*B*) Structure of the *Sp8* gene and the targeting vector. Green boxes (exons), blue box (zinc finger domain). Restriction sites: E, *Eco*RI; B, *Bam*HI; B2, *Bgl*II. (*C*) Southern blot analysis of wild-type (Wt) and *lgl* mutant DNA. The blot was hybridized with a 435-bp *Sp8* cDNA fragment containing sequences found within exon 2 and the beginning of exon 3. Arrowhead indicates the *Eco*RI fragment containing the coding region. (*D–J*) Whole mount and sectioned *in situ* hybridization using an *Sp8* riboprobe. (*D–F* and *H–J*) Wild-type embryos. (*D*) Expression is detected in the neuroepithelium at E8.5. (*E*) On E9.0, expression is heavy around the posterior neuropore/tailbud (red arrowhead) and is first evident in the forelimb (Fl) AER precursor. (*F* and *H*) By E10.5, expression is detectable in the telencephalon (T), dorsal and ventral forelimb ectoderm, AER (blue arrowhead), hindlimb (Hl) AER precursor, tail (red arrowhead), medial and lateral nasal processes, isthmus, and ventral spinal cord. H, heart. (*G*) $lgl^{-/-}$ embryo showing reduction in the level of expression in the forelimb AER, lateral and medial nasal processes, isthmus (red arrow), and the absence of expression in the hindlimb bud AER precursor. (*I* and *J*) On E12.5, expression is detected at the midbrain (Mb)/hindbrain (Hb) border, in the olfactory epithelium (OE) and the ventral thalamus (VT). Notably, *Sp8* is expressed in the olfactory bulb primordia (*J*, arrowhead).

Swiss mice or germ line *Cre* mice (20). PCR genotyping was performed on genomic DNA isolated from either embryonic yolk sacs or fetal visceral tissue. The endogenous allele was detected by using the primer pair 5′-TCCTCCCACGAGTGTAATGCTCAG-3′ and 5′-GCGTTCTTTCCCCCAACTTC-3′ under cycling conditions of 95°C for 30 s, 63°C for 30 s, and 72°C for 1 min. The recombined null allele was detected by using the primer pair 5′-CCACAGCCTCTTCAAAGTTCCG-3′ and 5′-GCGAGTAAGTTTTTCCCTCCTGG-3′ under cycling conditions of 95°C for 30 s, 60°C for 30 s, and 72°C for 1 min. Mice from two distinct targeted embryonic stem cell clones were studied and found to give identical phenotypes.

***In Situ* Hybridization.** A *Not*I/*Apa*I fragment of the *Sp8* cDNA was used for whole mount and sectioned *in situ* assays. Antisense riboprobes were kindly provided by Gail Martin (University of California, San Francisco) (*Fgf8*), Alexandra Joyner (New York University School of Medicine, New York) (*En1*), Robert Maxson (University of Southern California, Los Angeles) (*Msx2*), and Allan Bradley (Sanger Center, Cambridge, U.K.) (*p63*). Whole mount and sectioned *in situ* hybridization assays were performed as described (6, 21).

Skeletal Preparation. Alizarin red and alcian blue skeletal staining was performed as described (22).

Nile Blue Sulfate Staining. Dissected embryos were placed in Nile blue sulfate (1:20,000) in PBS for 15 min, rinsed in PBS for 30 min, and immediately photographed.

Results and Discussion

Release of the human 7p15–21 genomic sequence revealed the linkage of *Sp4* with *Sp8* in a region syntenic to the *lgl* transgene insertion. In the mouse, *Sp4* and *Sp8* are separated by ≈545 kb and arranged with their promoters facing each other (Fig. 1*A*), similar to the *Sp2–Sp6* and *Sp1–Sp7* gene pairs. Although the entire *Sp4* gene is deleted from the *lgl* genome, Southern blot analysis indicated that the *Sp8* coding region is intact (Fig. 1*C*). Additional PCR and Southern analysis positioned the transgene integration site ≈80 kb upstream of the *Sp8* coding region (data not shown).

The *Sp8* gene consists of two 5′ UTR exons and a third exon containing all of the coding and 3′ UTR sequences (Fig. 1*B*). This structure was determined by comparison of the mouse genomic sequence with an RT-PCR-derived *Sp8* cDNA from E10 mouse embryos as well as RIKEN and EST clones, EST BB663595 and the Fantom-DB clone 5730507L14 (NCBI accession no. AK030745) (23). This genomic structure closely resembles that observed for the *Sp5, 6*, and *7* genes (18, 19, 24).

The murine and human (NCBI accession no. NM_182700) *Sp8* cDNAs encode highly conserved proteins of 486 and 466 aa, respectively, with 97% identity. The human protein includes an additional 18 amino acids at the N terminus; the last four of these amino acids comprise the beginning of the conserved "Sp box" sequence TPLAMLAATCNKIGSP present in other family members (18). The mouse protein contains an additional 42-aa insertion after amino acid 103. Like other members of the Sp family, the buttonhead and the highly conserved zinc finger domains are at the C terminus (13, 18). In Sp8, these domains are most homologous to the *Drosophila* protein D-Sp1 and murine Sp7 (data not shown) (12, 19). Variability exists at the N termini, where Sp1–4 all possess large activation domains, whereas Sp8, like Sp5, 6, and 7, have significantly smaller domains of unknown function (13).

Sp8 expression during embryogenesis is distinct from other Sp family members (13, 18, 19, 24, 25). In E8 embryos, *Sp8* was expressed in the forming neural tube. On E9–10, localized expression was detected at the telencephalic midline, mid-hindbrain junction, ventral spinal cord, posterior neuropore, genital tubercle, tail bud, and lateral and medial nasal processes (Fig. 1 *D–H*). In the fore- and hindlimb buds, expression was observed in the AER precursor cells/AER and in the adjacent dorsal and ventral limb ectoderm (Fig. 1 *E*, *F*, and *H*). Notably, a dramatic reduction in *Sp8* expression in the lateral and medial nasal processes, forebrain, limbs, and tail bud was observed in E10–11 $lgl^{-/-}$ embryos (Fig. 1*G* and data not shown). At E12.5, *Sp8* expression remained in the mid-hindbrain boundary, the olfactory epithelia, and telencephalic midline and included the primordia of the olfactory bulbs (Fig. 1 *I* and *J*), which are missing in *lgl* mutants (9). Expression in the olfactory bulbs at later stages (e.g., E16.5, data not shown) was also evident. The reduced expression of *Sp8* in multiple sites of malformation in

Table 1. Phenotype comparison of *lgl*$^{-/-}$, *lgl*$^{+/-}$/*Sp8*$^{+/-}$, and *Sp8*$^{-/-}$ fetuses

Genotype	Forelimb malformations		Cranial malformations		Caudal malformations	
	Missing/dysplastic radius	Adactyly or monodactyly	Encephalocoeles	Exencephaly	Curled/bifurcated tail or vertebral fusions	Spina bifida/absent tail
lgl$^{-/-}$	4/36 (11%)	5/36 (14%)	10/18 (56%)	1/18 (6%)	7/18 (39%)	0/18 (0%)
lgl$^{+/-}$/Sp8$^{+/-}$	27/54 (50%)	38/54 (70%)	7/27 (26%)	16/27 (59%)	23/27 (85%)	0/27 (0%)
Sp8$^{-/-}$	22/22 (100%)	22/22 (100%)	0/11 (0%)	10/11 (91%)	0/11 (0%)	11/11 (100%)

the *lgl* mutant suggested that integration of the *lgl* transgene may have inactivated a distant regulatory element or that the hypermethylation associated with this transgene might have spread to flanking sequences repressing *Sp8* expression (26).

The interesting expression pattern of *Sp8* in the limb and craniofacial regions suggested that the observed severe reduction of *Sp8* expression in *lgl* mutants was responsible for their limb and craniofacial abnormalities. To determine *Sp8* function in these tissues, we targeted *loxP* sequences into the second intron and the 3′ UTR (Fig. 1*B*). *Sp8*$^{loxP/+}$ mice were mated to mice having germ-line *Cre* expression resulting in deletion of all *Sp8* coding sequences as well as the *Neo* selectable marker. The resulting *Sp8*$^{+/-}$ mice were normal.

We performed a complementation test by interbreeding *lgl*$^{+/-}$ and *Sp8*$^{+/-}$ mice to make *lgl*$^{+/-}$/*Sp8*$^{+/-}$ double heterozygotes. The resulting mice showed hindlimb malformations similar to those observed in *lgl*$^{-/-}$ mutants, with only the femur present. In addition, the forelimb and craniofacial malformations of double heterozygotes were more severe than for *lgl*$^{-/-}$ mutants (Table 1 and Fig. 2), thereby confirming a role for *Sp8* in these aspects of the *lgl*$^{-/-}$ phenotype.

To further define the developmental functions of *Sp8*, we interbred *Sp8*$^{+/-}$ mice to make *Sp8*$^{-/-}$ progeny. Like *lgl*$^{-/-}$ and *lgl*$^{+/-}$/*Sp8*$^{+/-}$, *Sp8*$^{-/-}$ individuals lacked hindlimb structures distal to the femur (Fig. 2 *E–H*). However, the complete absence of *Sp8* led to more severely affected forelimbs in which the radius and entire autopod were absent and the ulna was severely truncated (Table 1 and Fig. 2 *A–D* and *L*).

An effect of *Sp8* gene dosage was observed not only in limb morphogenesis but also in closure of the neural tube. The neural tube defects, exencephaly and spina bifida, were both observed in nearly all *Sp8*$^{-/-}$ fetuses (Fig. 2*L*, Table 1). In contrast, only 85% of the *lgl*$^{+/-}$/*Sp8*$^{+/-}$ fetuses had neural tube closure defects, with 59% exhibiting exencephaly and 26% possessing encephalocoeles. These defects were least evident in *lgl*$^{-/-}$ fetuses, with 56% exhibiting encephalocoeles and 6% exencephaly, with or without facial clefting (Table 1). Skeletal examinations indicated that there was a gene dosage related retardation or loss of cranial skeletal bones when comparing *Sp8*$^{-/-}$ to *lgl*$^{+/-}$/*Sp8*$^{+/-}$ perinates that included the frontal, parietal, nasal, premaxilla, and maxilla anteriorly as well as the supraoccipital posteriorly.

In mice, the neural tube defects spina bifida, split face, exencephaly, and rachischisis are caused by failure of neural tube closure along one of four zones of the neural tube. Although a number of mouse models exhibit exencephaly with or without spina bifida, in only a few of these is the exencephaly the result of a failure in closure at position 3, the anterior neuropore (for review see ref. 27). The exencephaly resulting from lowered or absent *Sp8* expression is attributable to a defect in anterior neuropore closure. In murine embryos, the anterior neuropore is normally closed by E9 of gestation (28) but remains open in E9.5 and older *Sp8*$^{-/-}$ embryos as emphasized by continued expression of *Fgf8* in a ring of cells surrounding the open anterior neuropore (Fig. 2 *I* and *J*). Whole mount *in situ* hybridizations on E10–11 embryos with the telencephalon-specific probe *Bf1* indicated that the forebrain protrudes progressively through the open anterior neuropore resulting in the exencephalic phenotype at E13 and later (Fig. 2 *I–L*).

Interestingly, a relationship between exencephaly and methylation has previously been postulated based on the observations that targeted mutation of the *de novo* methylase *Dnmt3b* results in exencephaly, methionine supplementation is necessary in whole embryo culture to prohibit exencephaly, and that exencephaly is often more frequently observed in females than males (for review see ref. 27). One hypothesis is that methylation of the inactivated X-chromosome in females depletes the available methylation pool reducing the normal amount of DNA, protein, and lipid methylation events. Notably, GC-rich regions are the targets of DNA methylases and also contain DNA-binding sites for members of the Sp family of transcription factors. Further-

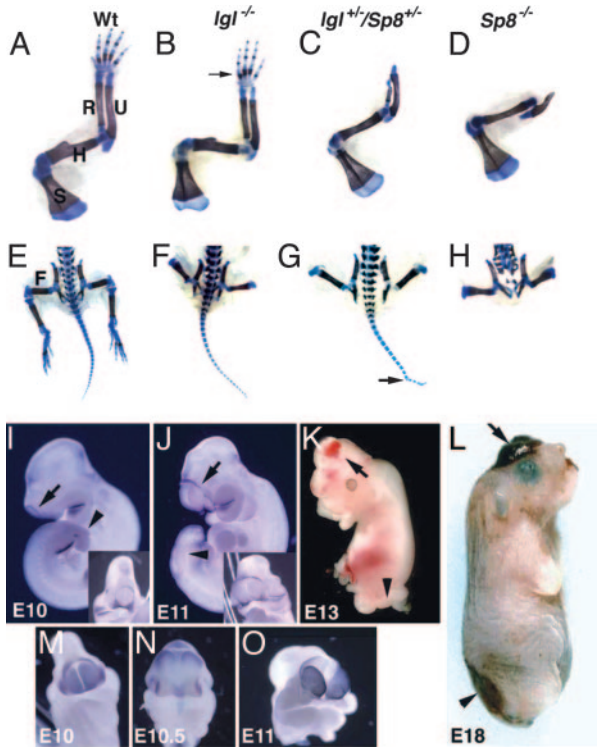

Fig. 2. Malformations in *Sp8* mutants. (*A–H*) Alizarin red and alcian blue limb skeletal analysis of E18 fetuses. (*A–D*) Forelimb skeletons. (*A*) S, scapula; H, humerus; R, radius; U, ulna. Arrow in *B* indicates absence of digit 1. (*C* and *D*) The humerus forms normally; however, the ulna is distally truncated. The radius is dysplastic (*C*) or absent (*D*) and the autopod is absent. (*E–H*) Caudal portion of fetuses. (*E*) F, femur. (*F–H*) Structures distal to the femur are absent. (*G*) Tail vertebral fusions (arrow). (*H*) In the *Sp8*$^{-/-}$ fetus, sacral and caudal vertebrae are absent and the lumbar vertebrae are disorganized and abnormal. (*I–M* and *O*) *Sp8* null embryos at the ages indicated. (*N*) Wild type. (*I–L*) Arrows indicate open anterior neuropore/exencephaly. Arrowheads indicate open posterior neuropore/spina bifida. (*I* and *J*) Whole mount *in situ* with *Fgf8* riboprobe arrows indicate ring of cells around open anterior neuropore. (*Inset*) Frontal view. (*M–O*) Whole mount *in situ* with *Bf1* riboprobe emphasizing progression of telencephalon tissue through open anterior neuropore.

DEVELOPMENTAL BIOLOGY

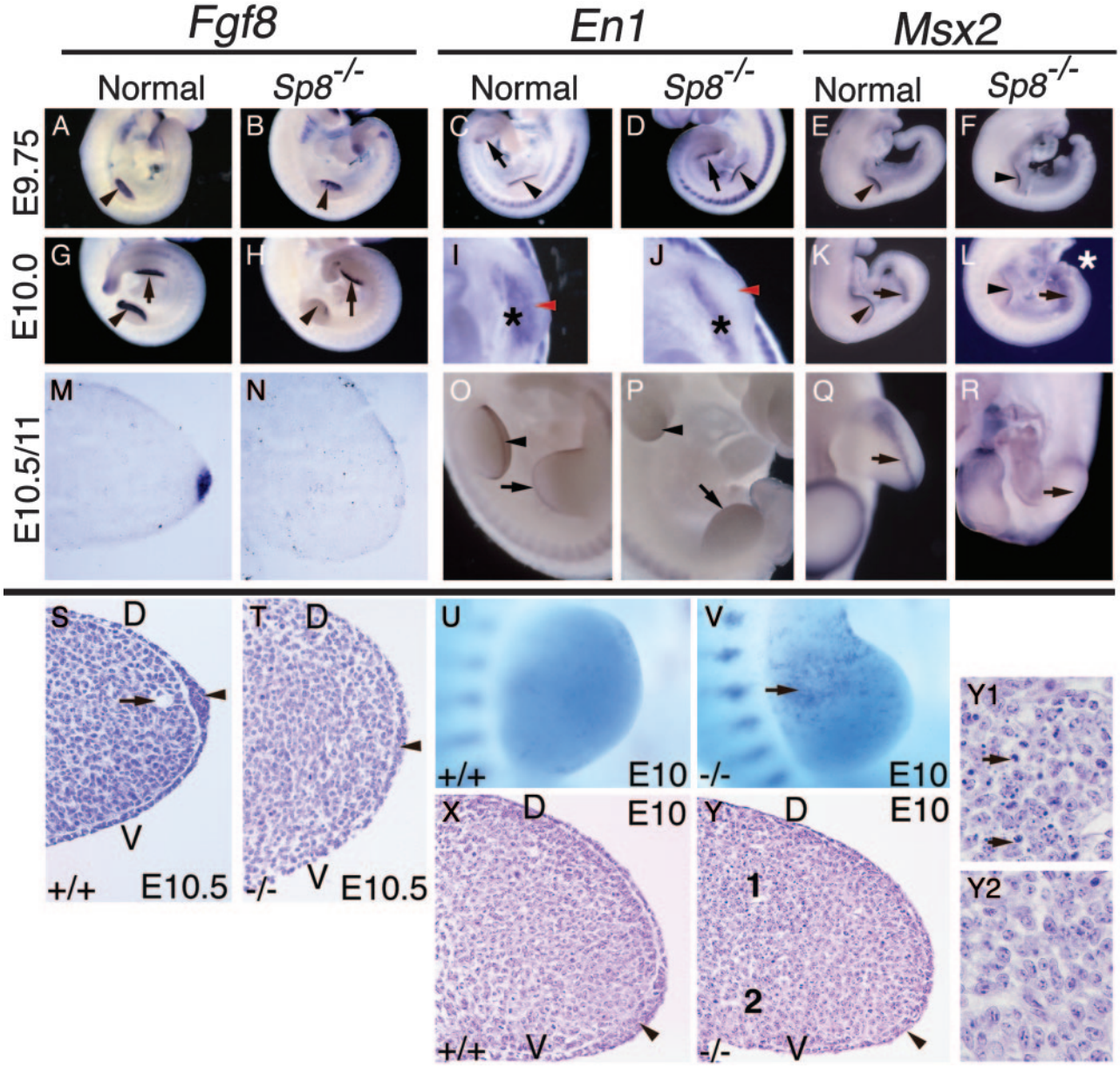

Fig. 3. Disruption in AER morphogenesis in *Sp8* null embryos. Embryo ages, genotypes, and probes used in the whole mount and section *in situ* hybridizations are indicated. Black arrowheads in *A–Y* indicate forelimb AER precursor/AER. Black arrows in *A–R* indicate hindlimb AER precursor. Note induction and subsequent loss of *Fgf8, Msx2*, and *En1* expression in the fore and hindlimb buds of $Sp8^{-/-}$ embryos. (*I* and *J*) Black asterisks indicate ventral ectoderm expression of *En1*, red arrowheads indicate normal position of *En1* expressing AER precursor cells and absence of expression in $Sp8^{-/-}$ forelimb bud. (*L*) White asterisk indicates truncated tail bud and open everted neural tissue adjacent to hindlimb buds. (*P*) Note the absence of *En1* expression at distal tips of limb buds and in somites adjacent to the hindlimbs. (*Q* and *R*) Hindlimb buds, apical view. (*S, T, X, Y, Y1*, and *Y2*). Hematoxylin and eosin-stained 6-μm paraffin sections cut across the anterior/posterior axis of the forelimb. Arrowheads in *S, T, X*, and *Y* indicate AER precursor/AER. Arrow in *S* indicates marginal venous sinus. (*U* and *V*) Nile blue sulfate cell death staining, note punctate blue staining in anterior proximal region of $Sp8^{-/-}$ limb indicated by arrow in *V*. (*Y*) Note presence of pyknotic nuclei in dorsal proximal region of limb seen at higher magnification in *Y1* compared with the proximal ventral mesoderm presented in *Y2*. D, dorsal; V, ventral.

more, human supplementation with folic acid has been credited with reducing the incidence of neural tube defects and two genes in the folate pathway require the presence of Sp binding sites within their promoters for their expression (29, 30).

In caudal regions of the embryo, $Sp8^{-/-}$ progeny all exhibit spina bifida accompanied by complete absence of the tail (Table 1 and Fig. 2 *H* and *L*). $Lgl^{+/-}/Sp8^{+/-}$ and $lgl^{-/-}$ fetuses never exhibit spina bifida but do have an *Sp8* gene dosage-dependent incidence of tail malformations, 85% and 39%, respectively. Fusion of the caudal vertebrae is the most commonly observed malformation (Fig. 2*G*), although one bifurcated tail tip was noted.

Like the curly tail mouse mutant, the lumbosacral spina bifida observed in $Sp8^{-/-}$ fetuses is caused by a defect in primary neurulation (31). Posterior neuropore closure is normally completed by E10 at a position between somites 32 and 34 in the mouse, whereas secondary neurulation doesn't begin until somite 32 (32). In the $Sp8^{-/-}$ embryos, posterior neuropore defects are first evident on E9.5 as a failure of the posterior neuropore to close and eversion of the posterior neural folds. By E10, a lack of closure paralleling somites 25–31 is present, the tail bud is not evident, and somite formation posterior to the emerging hindlimbs has ceased (Figs. 2*I* and 3 *F*, *H*, and *L*). By

E11, the patterning of somites adjacent to the hindlimbs is disrupted as evidenced by the lack of *En1* expression (Fig. 3*P*).

In the emerging limb bud, *Sp8* is coexpressed throughout the limb ectoderm with *Wnt3*, *p63*, and *Fgfr2b*. However, in the absence of *Sp8*, the humerus and femur do form, whereas all hindlimb structures are absent upon removal of *Wnt3* (1), *β-catenin* (1), *p63* (33, 34), *Bmpr1a* (2), or *Fgfr2b* (4, 5) expression from the limb. Furthermore, the expression of *Fgf8* and other markers of the AER precursor population was not detectable in the ventro-distal ectoderm of emerging limb buds of *Fgfr2b, Bmpr1a*, or β-catenin-deficient embryos. We have examined this cell population in the fore- and hindlimb buds of $lgl^{+/-}/Sp8^{+/-}$ and $Sp8^{-/-}$ embryos on E9–11 of gestation histologically and by whole mount and section *in situ* hybridization. In stage 1 fore- and hindlimb buds, *Fgf8*, *En1*, *Msx2*, and *p63* expression was initiated, but the expression of these genes was rapidly lost and an AER failed to form (Fig. 3 *A–T*, data not shown). Although *En1* expression in the disto-ventral AER precursor was undetectable in stage 2 and older $Sp8^{-/-}$ limb buds, expression was detectable in the proximo-ventral ectoderm (Fig. 3 *I* and *J*), confirming initial establishment of the dorsal/ventral axis in the $Sp8^{-/-}$ limb bud. In addition to being expressed in the AER precursor, *p63* is also normally expressed by the dorsal and ventral limb ectoderm (33, 34). This expression in non-AER ectoderm was unaffected in $Sp8^{-/-}$ embryos (data not shown). By E10.5/11 *Msx2* expression in the fore- and hindlimb buds, respectively, was undetectable in the AER precursor cells. Small expression domains were, however, transiently detectable in the anterior and posterior mesoderm (Fig. 3 *Q* and *R*).

Because an AER can still form in the absence of both Fgf8 and Fgf4 (35), we also evaluated AER formation histologically in the forelimb buds of E10 and E10.5 $Sp8^{-/-}$ embryos. AER precursor cells were present as a thickened population of cells at E10 (Fig. 3 *X* and *Y*). At E10.5, a distinct AER has formed across the entire anterior posterior axis of nonmutant limbs (Fig. 3 *M* and *S*). In contrast, most of the apical ectoderm in $Sp8^{-/-}$ embryos is indistinguishable from adjacent dorsal and ventral ectoderm. A few regions of thickened ectoderm were observed in the very middle of some limb buds (Fig. 3*T*); however, neither *Fgf8* nor *Msx2* expression was detectable by section *in situ* hybridization within this population of cells at E10.5 (Fig. 3*N* and data not shown). Consistent with our conclusion that a functional AER fails to form, in all mutant limb buds examined there was no evidence of the marginal venous sinus in the distal limb mesoderm (Fig. 3*S*), a structure that forms in response to AER signaling.

Surgical removal of the ridge or a ridge lacking FGF signaling results in mesenchymal cell death (35–37). Cell death in $Sp8^{-/-}$ forelimb buds was assayed by staining with the vital dye Nile blue sulfate. Abnormal cell death was first evident in stage 1 forelimbs of E9.5 $Sp8^{-/-}$ embryos (data not shown). A prominent anterior, proximal zone of cell death was evident in stage 2–3 $Sp8^{-/-}$ limb buds on E10, whereas no cell death was observed in this region of wild-type littermates (Fig. 3 *U* and *V*). Histological sections confirmed the presence of pyknotic nuclei in an anterior, dorsal, proximal region of the $Sp8^{-/-}$ forelimb (Fig. 3 *Y* and *Y1*). This zone of cell death in $Sp8^{-/-}$ embryos is very similar to that observed in Fgf 4/8 double knockout limbs (35), but its location contrasts with that found in the distal mesenchyme after surgical removal of the AER (36, 37).

The observed early transient expression of *Fgf8* in $Sp8^{-/-}$ embryos is consistent with the ability of the limb buds to specify the most proximal limb skeletal elements (35). The initial induction of the AER precursor population expressing *Fgf8*, *Msx2*, and *En1* in $Sp8^{-/-}$ embryos is in agreement with our previous studies of $lgl^{-/-}$ hindlimb buds, which indicated that the AER precursor population was induced and expressed a variety of markers including *Fgf8*, *En1*, *Dlx2*, *Cd44*, *Bmp4*, *Cx43*, and *Msx2* (6). However, by stage 2, the expression of all of these markers was lost, the AER precursor cells failed to localize at the disto-ventral margin, and limb outgrowth subsequently ceased. As proposed in the AER induction model in Fig. 4, these observations show that *Sp8* functions downstream of molecules like Wnt3, β-catenin, and Bmpr1a in the signaling cascade leading to AER precursor induction. Our data indicate that Sp8 is required to maintain early AER genetic marker expression and also that developmental progression of the AER requires *Sp8* expression. Sp8 may be required to maintain expression of a key signaling molecule like Wnt3 or a component of the Wnt signaling pathway. Notably, like the limb, tail bud formation also depends on Wnt signaling (38, 39), and the tail bud is also a site of *Sp8* expression and dysmorphogenesis in $Sp8^{-/-}$ embryos.

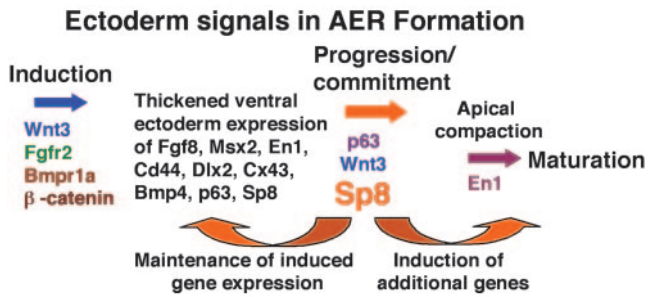

Fig. 4. Proposed model of genes involved in the process of AER formation. Only the genes in color have been implicated as being required for normal AER formation.

In summary, we have presented evidence indicating that *Sp8* is a key player in the genetic pathways that mediate limb outgrowth and neural tube closure. Unlike other genes involved in early AER formation, *Sp8* is critical for maintenance/progression of the induced AER precursor population to the disto-ventral margin of the limb. The observed anterior and posterior neural tube defects indicate that *Sp8* is also required in the process of neuropore closure. Because neural tube defects are one of the most common human malformations observed (40) and high levels of amino acid identity are observed between the murine and human *Sp8* orthologues, *Sp8* represents a new candidate gene for these devastating birth defects. There are numerous case reports of chromosomal excess and deficiency that include 7p21 and are associated with craniofacial, limb, CNS, urogenital, cardiovascular, and gastrointestinal malformations (41, 42). Future studies will be needed to distinguish any involvement of *Sp8* in these human syndromes and to define the genes regulated by *Sp8* that are responsible for AER maturation and neuropore closure in the mouse.

This work would not have been possible without the extensive studies of the transgene integration site performed by Dr. Dorothy Supp and the technical assistance of Brad Huntsman. All animal protocols were approved by the Institutional Animal Care and Use Committee in accordance with National Institutes of Health guidelines. This work was funded by National Institutes of Health Grant HD24517.

1. Barrow, J. R., Thomas, K. R., Boussadia-Zahui, O., Moore, R., Kemler, R., Capecchi, M. R. & McMahon, A. P. (2003) *Genes Dev.* **17,** 394–409.
2. Ahn, K., Mishina, Y., Hanks, M. C., Behringer, R. R. & Crenshaw, E. B. I. (2001) *Development (Cambridge, U.K.)* **128,** 4449–4461.
3. Min, H., Danilenko, D. M., Scully, S. A., Bolon, B., Ring, B. D., Tarpley, J. E., DeRose, M. & Simonet, W. S. (1998) *Genes Dev.* **12,** 3156–3161.
4. Xu, X., Weinstein, M., Li, Cuiling, Naski, M., Cohen, R. I., Ornitz, D. M., Leder, P. & Deng, C. (1998) *Development (Cambridge, U.K.)* **125,** 753–765.
5. Moerlooze, D. L., Spencer-Dene, B., Revest, J.-M., Hajihosseini, M., Rosewell, I. & Dickson, C. (2000) *Development (Cambridge, U.K.)* **127,** 483–492.
6. Bell, S. M., Schreiner, C. M. & Scott, W. J. (1998) *Mech. Dev.* **74,** 41–50.

7. Loomis, C. A., Kimmel, R., Tong, C.-X., Michaud, J. & Joyner, A. L. (1998) *Development (Cambridge, U.K.)* **125,** 1137–1148.
8. McNeish, J., Scott, W. & Potter, S. (1988) *Science* **241,** 837–839.
9. McNeish, J, Thayer, J., Walling, K., Sulik, K., Potter, S. & Scott, W. (1990) *J. Exp. Zool.* **253,** 151–162.
10. Supp, D. M., Witte, D. P., Branford, W. W., Smith, E. P. & Potter, S. S. (1996) *Dev. Biol.* **176,** 284–299.
11. Supp, D. M., Brueckner, M., Kuehn, M. R., Witte, D. P., Lowe, L. A., McGrath, J., Corrales, J. & Potter, S. S. (1999) *Development (Cambridge, U.K.)* **126,** 5495–5504.
12. Schock, F., Purnell, B. A., Wimmer, E. A. & Jackle, H. (1999) *Mech. Dev.* **89,** 125–132.
13. Bouwman, P. & Philipsen, S. (2002) *Mol. Cell. Endocrinol.* **195,** 27–38.
14. Marin, M., Karis, A., Visser, P., Grosveld, F. & Philipsen, S. (1997) *Cell* **89,** 619–628.
15. Bouwman, P., Gollner, H., Elsasser, H. P., Eckhoff, G., Karis, A., Grosveld, F., Philipsen, S. & Suske, G. (2000) *EMBO J.* **19,** 655–661.
16. Gollner, H., Dani, C., Phillips, B., Philipsen, S. & Suske, G. (2001) *Mech. Dev.* **106,** 77–83.
17. Nguyen-Tran, V. T., Kubalak, S. W., Minamisawa, S., Fiset, C., Wollert, K. C., Brown, A. B., Ruiz-Lozano, P., Barrere-Lemaire, S., Kondo, R., Norman, L. W., *et al.* (2000) *Cell* **102,** 671–682.
18. Harrison, S. M., Houzelstein, D., Dunwoodie, S. L. & Beddington, R. S. (2000) *Dev. Biol.* **227,** 358–372.
19. Nakashima, K., Zhou, X., Kunkel, G., Zhang, Z., Deng, J. M., Behringer, R. R. & Crombrugghe, B. (2002) *Cell* **108,** 17–29.
20. Lakso, M., Pichel, J. G., Gorman, J. R., Sauer, B., Okamoto, Y., Lee, E., Alt, F. W. & Westphal, H. (1996) *Proc. Natl. Acad. Sci. USA* **93,** 5860–5865.
21. Toresson, H., Mata de Urquiza, A., Fagerstrom, C., Perlmann, T. & Campbell, K. (1999) *Development (Cambridge, U.K.)* **126,** 1317–1326.
22. Kuczuk, M. H. & Scott, W. J. (1984) *Teratology* **29,** 427–435.
23. The FANTOM Consortium and the RIKEN Genome Exploration Research Group Phase I and II Team (2002) *Nature* **420,** 563–573.
24. Scohy, S. Gabant, P., Reeth, T. V., Hertveldt, V., Dreze, P.-L., Vooren, P. V., Riviere, M., Szpirer, J. & Szpirer, C. (2000) *Genomics* **70,** 93–101.
25. Treichel, D., Becker, M.-B. & Gruss, P. (2001) *Mech. Dev.* **101,** 175–179.
26. Singh, G., Supp, D. M., Schreiner, C., McNeish, J., Merker, H. J., Copeland, N. G., Jenkins, N. A., Potter, S. S. & Scott, W. (1991) *Genes Dev.* **5,** 2245–2255.
27. Juriloff, D. M. & Harris, M. J. (2000) *Hum. Mol. Genet.* **9,** 993–1000.
28. Sakai, Y. (1989) *Anat. Rec.* **223,** 194–203.
29. Park, K. K., Rue, S.-W., Lee, I.-S., Kim, H.-C., Lee, I.-K., Ahn, J. D., Kim, H.-S., Yu, T.-S., Kwak, J.-Y., Henitz, N. H., *et al.* (2003) *Biochem. Biophys. Res. Commun.* **306,** 239–243.
30. Hao, H., Qi, H. & Ratnam, M. (2003) *Blood* **101,** 4551–4560.
31. Schoenwolf, G. C. (1984) *Am. J. Anat.* **169,** 361–374.
32. Copp, A. J. & Brook, F. A. (1989) *J. Med. Genet.* **26,** 160–166.
33. Mills, A. A., Zheng, B., Wang, X.-J., Vogel, H., Roop, D. R. & Bradley, A. (1999) *Nature* **398,** 708–713.
34. Yang, A., Schweitzer, R., Sun, D., Kaghad, M., Walker, N., Bronson, R. T., Tabin, C., Sharpe, A., Caput, D., Crum, C. & McKeon, F. (1999) *Nature* **398,** 714–718.
35. Sun, X., Mariani, F. V. & Martin, G. R. (2002) *Nature* **418,** 501–508.
36. Rowe, D. A., Cairns, J. M. & Fallon, J. F. (1982) *Dev. Biol.* **93,** 83–91.
37. Dudley, A. T., Ros, M. A. & Tabin, C. J. (2002) *Nature* **418,** 539–544.
38. Takada, S., Stark, K. L., Shea, M. J., Vassileva, G., McMahon, J. A. & McMahon, A. P. (1994) *Genes Dev.* **8,** 174–189.
39. Pinson, K. I., Brennan, J., Monkley, S., Avery, B. J. & Skarnes, W. C. (2000) *Nature* **407,** 535–538.
40. Mulinaire, J. & Erickson, J. D. (1997) *Teratology* **56,** 17–18.
41. Ahrens, Y. H. J. M., Toutain, A., Engelen, J. J. M., Offermans, J. P. M., Hamers, A. J. H., Schrander, J. J. P., Pulles-Heintzberger, C. F. M. & Schrander-Stumpel, C. T. R. M. (2000) *Genet. Couns.* **11,** 347–354.
42. Hoover-Fong, J. E. Cai, J., Cargile, C. B., Thomas, G. H., Patel, A., Griffin, C. A. & Jabs, E. W. (2003) *Am. J. Med. Genet.* **117A,** 47–56.